Complex magnetism in Ni3TeO6-type Co3TeO6 and high-pressure polymorphs of Mn3-xCoxTeO6 solid solutions

Complex magnetism in Ni_3TeO_6-type Co_3TeO_6 and high-pressure polymorphs of $Mn_{3-x}Co_xTeO_6$ solid solutions.

Elena Solana-Madruga,[a,b] Cintli Aguilar-Maldonado,[a] Clemens Ritter,[c] Marielle Huvé[a], Olivier Mentré[a], J.Paul Attfield[b] and Ángel M. Arévalo-López[a]*.

Supplementary Text:

- Experimental Methods:

The precursor oxides were prepared at 1270 K by solid state synthesis method from the stoichiometric mixture of binary Mn_3O_4, Co_3O_4 and TeO_2 oxides. These were then packed into Pt capsules and pressed to 8-15 GPa using a Walker-type multianvil module. The samples were then heated at 1173 K for 20 minutes, quenched and slowly depressurised. Note higher pressures are needed to stabilise larger amounts of smaller Co^{2+} in the large cuboctahedral void of the DPv structure (0.90 Å vs. 0.96 Å for Mn^{2+} in 8-fold coordination) [1]. For this reason, the presence of secondary NTO phase in the x = 1.5 compound at 10 GPa motivated the use of 12, 13 and 15 GPa for the synthesis of x = 2, 2.5 and 3 respectively. As discussed in the main text, the use of 15 GPa allowed the characterisation of secondary DPv-Co_3TeO_6, suggesting the accessibility of this polymorph for the complete system: traces of DPv phase are observed in x = 2 and 2.5, but the small proportion and the relatively low resolution of the diffraction data did not allow for their full refinement and further studies will be addressed for the study of pure phases. Note the refined occupancies for the x = 2 compound reveal an overall $Mn_{1.25}Co_{1.75}TeO_6$ composition, in keeping with the minor amounts of secondary CoO (4.74%) found. This reflects the higher stability of Mn^{2+} and the need for higher synthesis pressures to stabilize fully stoichiometric $MnCo_2TeO_6$. The higher pressures used for compositions with larger Co content yield to the aimed $Mn_{0.5}Co_{2.5}TeO_6$ and Co_3TeO_6 within error, thus justifying the results of the x = 2 compound as representative in the series.

Bulk magnetic behaviour was studied from FC-ZFC magnetic susceptibility and hysteresis loops measured at several temperatures up to $\pm$ 9 T using a PPMS 9T Dynacool Quantum Design. (SF1)

Synchrotron X-ray diffraction data were collected in the 2θ 0-180^0 angular range at I11 beamline at Diamond using λ = 0.826514 Å. (SF2)

The presence of a possible superstructure in Co_3TeO_6 was checked and ruled out by means of selected-area electron diffraction (SAED) (SF3). HP-Co_3TeO_6 was ground in butyl alcohol and ultrasonically dispersed. A few drops of the resulting suspension were deposited on a carbon-coated grid. SAED experiments were performed with a FEI TechnaiG2 20 microscope operating at 200 kV, fitted with an X-ray energy-dispersive spectroscopy (XEDS) microanalysis system. The atomic ratio of the metals was determined by XEDS analyses, finding good agreement between analytical and nominal composition in the crystals.

Neutron Powder Diffraction (NPD) was collected at D20 beamline at the Institut Laue- Langevin. High-resolution data were collected at 300 K for accurate structural characterisation of HP-Co_3TeO_6 using λ = 1.54 Å. Additional scans were collected for all samples using λ = 2.41 Å at selected temperatures above and below the magnetic transitions according to their bulk mangetisation and at 1.5 K. Short scans were measured on ramping upon warming the samples from base temperature to study the thermal evolution of their magnetic structures. All collected diffraction patterns were Rietveld refined with FullProf Suite. Magnetic symmetry analysis was performed using BasIreps.[2]

- Magnetic symmetry analysis and magnetic structure refinements

a) Magnetic symmetry analysis of HP-Co_3TeO_6 with BasIreps using propagation vectors [0 0 0] and [0 0 k_z] are summarised in supplementary Table S1. The former describes collinear AFM structures with the spins lying along the *c* axis (Γ_1) or into the *ab* plane (Γ_2 and Γ_3). The Ireps allowed by the incommensurate propagation vector describe either a sine wave (Γ_1) or a complex helical structure (Γ_2 and Γ_3) with clockwise and counterclockwise rotation of the spins. Note the powder nature of the sample masks any difference between these two helical models.

The main (003) magnetic peak and their satellites indicates the main contribution to the magnetic moments lie on the *ab* plane. According to this, Γ_2 was selected for both (k_0 and k_z) magnetic contributions. Their combination originates an elliptical helix as described in the main text. The magnetic component involved in the 3 Co^{2+} magnetic sites was constrained in both bases for the refinement of the 40 K – 80 K difference pattern. The refinement of 1.5 K – 80 K, with the additional k_{z2} contribution, was subjected to the same constraints. In addition, the m_x component of the circular helix described by the k_{z2} phase was also constrained to that of the k_{z1} elliptical helix phase.

HP-$Mn_{0.5}Co_{2.5}TeO_6$ and HP-$MnCo_2TeO_6$ magnetic structures were fitted using the same Ireps and constraints (SF4). Note their cation order could be expected to induce different moments in Co1 site (Mn preferred). The independent refinement of Mn and Co – site moments was considered but the sequential refinements were unstable. The refined moments were therefore constrained together.

Their 2D thermodiffraction shown in SF5 reveals no temperature dependence of their k_z vectors.

b) Magnetic symmetry analysis of HP-Mn_2CoTeO_6 with BasIreps using propagation vector [0 0 0] allows for the Ireps shown in Table S2. As in the case of the related Mn_3TeO_6–II analysis with k = [½ 0 ½] [3], the possible Ireps describe 3 different types of AFM order with the spins confined to the *ac* plane and one were the AFM interactions are aligned along the *b* axis. All possible AFM models were tested and the best solution Γ_1 was selected. The independent refinement of m_x and m_z components refine within error to [201] direction for both A and B sites. According to this and coherently with the magnetic structure reported for Mn_3TeO_6-II, both spins were constrained to this direction (SF4). Relative phase proportions of k = [½ 0 ½] and k_0 phases was refined for HP-$Mn_{2.5}Co_{0.5}TeO_6$ (SF4) using a linear constraint.

The refinement of the magnetic structures for the DPv and NTO phases of HP-$Mn_{1.5}Co_{1.5}TeO_6$ was performed using the same constraints as for all other related phases in the system from the 1.5 K – 40 K and 40 K – 80 K difference patterns respectively (SF4).

c) Sequential refinements of the raw data collected every 1 K between 3 and 80 K on NTO-Co_3TeO_6 for determining the thermal evolution of its magnetic moments and propagation vectors was performed using the 1.5 K (k_0+k_{z1} and k_{z2}) and 40 K (k_0+k_{z1}) models in the 3 – 23.5 K and 23.5 – 60 K temperature regions respectively. The relative proportion of both magnetic phases in the 3 – 23.5 K temperature range was fixed for stability of the refinements, though test fits with fixed magnetic moments from 1.5 K – 80 K difference pattern converge to nearly 50 % of each phase at all temperatures with a quick emergence of the k_{z2} phase right below T_{N2}.

Sequential refinements of all other phases were performed against raw NPD data following the same constraints as their low temperature refinements. All compounds show coherent evolution of their magnetic moments.

Table S1. Irreducible representations (Irep) and basis vectors (Real and Imaginary components) from the magnetic symmetry analysis of NTO-Co_3TeO_6 (*R3*) with propagation vectors [0 0 0] and [0 0 k_z].

Symm	Γ_1	Γ_2	Γ_3
x, y, z			
Bas R	0 0 1	1 0 0	1 0 0
Bas I	0 0 0	-0.5774 -1.1547 0	0.5774 1.1547 0

Table S2. Irreducible representations (Irep) and basis vectors from the magnetic symmetry analysis of HP-Mn_2CoTeO_6 (*P21/n*) with propagation vector [0 0 0]. Only real components are shown, since imaginary components are 0 for all basis vectors. Only Γ_1 and Γ_3 apply for magnetic B sites and only the two first rows of symmetries are basis for them.

Symm	Γ_1	Γ_2	Γ_3	Γ_4
x, y, z	100 010 001	100 010 001	100 010 001	100 010 001
-x+½, y+½, -z+½	-100 010 00-1	-100 010 00-1	100 0-10 001	100 0-10 00-1
-x, -y, -z	100 010 001	-100 0-10 00-1	100 010 001	-100 0-10 00-1
x+½, -y+½, z+½	-100 010 00-1	100 0-10 001	100 0-10 001	-100 010 00-1

Table S3. Atomic positions of HP-$Mn_{0.5}Co_{2.5}TeO_6$ from the Rietveld fit of 300 K SXRD data. S.G. *R3, a* = 5.22078(8) Å, *c* = 13.8318(3) Å. Co1 site z-coordinate was fixed as a reference for the cell origin. Mn/Co occupancies fixed from the refined values against NPD data. Cation and oxygen thermal factors constrained and fixed respectively for stability of the refinement.

Site	x	Y	z	B_{iso}(Å^2)	Occ(Mn/Co)
Co1 (3a)	0.0	0.0	0.062	0.52(1)	0.487/0.513
Co2 (3a)	0.0	0.0	0.2627(3)	0.52(1)	0.024/0.976
Co3 (3a)	0.0	0.0	0.5574(4)	0.52(1)	0.005/0.995
Te (3a)	0.0	0.0	0.7745(3)	0.52(1)	1.0
O1 (9b)	0.362(2)	0.046(2)	0.170(1)	0.24	1.0
O2 (9b)	0.335(3)	0.379(2)	0.344(1)	0.24	1.0

Table S4. Atomic positions of HP-$MnCo_2TeO_6$ from the Rietveld fit of 90 K NPD data. S.G. *R3, a* = 5.2294(2) Å, *c* = 13.873(1) Å. Co1 site z-coordinate was fixed as a reference for the cell origin. No 300 K SXRD data available. Thermal factors constrained for stability of the refinement. Note the refined occupancies reveal an overall $Mn_{1.25}Co_{1.75}TeO_6$ composition, in keeping with the minor amounts of secondary CoO (4.74%).

Site	x	Y	z	B_{iso}(Å^2)	Occ(Mn/Co)
Co1 (3a)	0.0	0.0	0.062	0.16(2)	0.952/0.048(3)
Co2 (3a)	0.0	0.0	0.286(2)	0.16(2)	0.100/0.900(4)
Co3 (3a)	0.0	0.0	0.450(3)	0.16(2)	0.201/0.799(3)
Te (3a)	0.0	0.0	0.692(1)	0.16(2)	1.0
O1 (9b)	0.331(1)	0.0663(8)	0.123(1)	0.16(2)	1.0
O2 (9b)	0.3172(9)	0.292(1)	0.288(1)	0.16(2)	1.0

Table S5. Atomic positions of the minor (11.6%) NTO phase of HP-$Mn_{1.5}Co_{1.5}TeO_6$ from the Rietveld fit of 300 K SXRD data. S.G. *R3, a* = 5.2767(1) Å, *c* = 13.8539(4) Å. Co1 site z-coordinate was fixed as a reference for the cell origin. Thermal factors fixed from NPD for stability of the refinement. Cation distribution fixed to ideal disordered Mn/Co. Their refined values from NPD suggest a Mn/Co inverted site preference, but it has been considered not reliable from our D20 data due to the low phase proportion.

Site	x	Y	z	B_{iso}(Å^2)	Occ(Mn/Co)
Co1 (3a)	0.0	0.0	0.062	0.21	0.5/0.5
Co2 (3a)	0.0	0.0	0.273(1)	0.21	0.5/0.5
Co3 (3a)	0.0	0.0	0.558(1)	0.21	0.5/0.5
Te (3a)	0.0	0.0	0.776(1)	0.21	1.0
O1 (9b)	0.302(4)	-0.044(4)	0.198(1)	0.9	1.0
O2 (9b)	0.311(4)	0.379(3)	0.360(1)	0.9	1.0

Table S6. Atomic positions of the main (88.4%) DPv phase of HP-$Mn_{1.5}Co_{1.5}TeO_6$ from the Rietveld fit of 300 K SXRD data. S.G. *P21/n, a* = 5.24840(5) Å, *b* = 5.35116(6) Å, *c* = 7.71821(7) Å and β = 90.5448(8) °. Mn/Co occupancies fixed from the refined values against NPD data.

Site	x	Y	z	B_{iso}(Å^2)	Occ (Mn/Co)
Te (2d)	0	0.5	0	0.37(2)	1
B (2b)	0.5	0	0	0.37(2)	0.164/0.836
A (4e)	0.5074(6)	0.4572(4)	0.2364(3)	0.41(5)	0.668/0.332
O1 (4e)	0.125(1)	0.593(1)	0.219(1)	0.1(1)	1
O2 (4e)	0.682(2)	0.685(1)	0.051(1)	0.1(1)	1
O3 (4e)	0.834(2)	0.219(2)	0.082(1)	0.1(1)	1

Table S7. Atomic positions of the DPv phase of HP-Mn_2CoTeO_6 from the Rietveld fit of 300 K SXRD data. S.G. *P21/n, a* = 5.25408(6) Å, *b* = 5.38753(8) Å, *c* = 7.74881(9) Å and β =90.5274(8) °. Mn/Co occupancies fixed from the refined values against NPD data. Oxygen thermal factors fixed for stability.

Site	x	Y	z	B_{iso}(Å^2)	Occ (Mn/Co)
Te (2d)	0	0.5	0	0.04(3)	1
B (2b)	0.5	0	0	0.76(7)	0.153/0.847
A (4e)	0.5110(5)	0.4506(3)	0.2380(3)	0.16(3)	0.847/0.153
O1 (4e)	0.125(1)	0.576(1)	0.226(1)	0.26	1
O2 (4e)	0.704(1)	0.692(1)	0.056(1)	0.26	1
O3 (4e)	0.836(1)	0.218(1)	0.079(1)	0.26	1

The low B_{iso} value resulting for Te sites could reflect either the low thermal vibration of this non-polarizable cation in a highly symmetric crystallographic site and/or the compensation against the relatively large values fixed for O.

Table S8. Atomic positions of the DPv phase of HP-$Mn_{2.5}Co_{0.5}TeO_6$ from the Rietveld fit of 300 K SXRD data. S.G. *P21/n, a* = 5.26942(9) Å, *b* = 5.4189(1) Å, *c* = 7.7766(1) Å and β = 90.457(1) °. Mn/Co occupancies fixed from the refined values against NPD data. Oxygen thermal factors fixed for stability.

Site	x	Y	z	B_{iso}(Å^2)	Occ (Mn/Co)
Te (2d)	0	0.5	0	0.06(3)	1
B (2b)	0.5	0	0	0.50(2)	0.505/0.495
A (4e)	0.5154(8)	0.4465(6)	0.2446(5)	0.6(1)	0.995/0.005
O1 (4e)	0.148(2)	0.592(2)	0.232(1)	0.19	1
O2 (4e)	0.709(2)	0.698(2)	0.058(1)	0.19	1
O3 (4e)	0.849(2)	0.206(2)	0.081(1)	0.19	1

The low B_{iso} value resulting for Te sites could reflect either the low thermal vibration of this non-polarizable cation in a highly symmetric crystallographic site and/or the compensation against the relatively large values fixed for O.

Table S9. Atomic positions of the minor (14.8%) DPv phase of HP-Co_3TeO_6 from the Rietveld fit of 300 K NPD data. S.G. *P21/n, a* = 5.115(1) Å, *b* = 5.421(1) Å, *c* = 7.354(2) Å and β = 90.68(2) °.

Site	x	Y	z	B_{iso}(Å^2)	Occ
Te (2d)	0	0.5	0	1.1(7)	1
CoB (2b)	0.5	0	0	1.1(7)	1
CoA (4e)	0.42(1)	0.37(1)	0.300(8)	1.1(7)	1
O1 (4e)	0.171(5)	0.581(4)	0.236(4)	0.9(3)	1
O2 (4e)	0.632(5)	0.530(4)	0.032(3)	0.9(3)	1
O3 (4e)	0.825(5)	0.160(4)	0.103(3)	0.9(3)	1

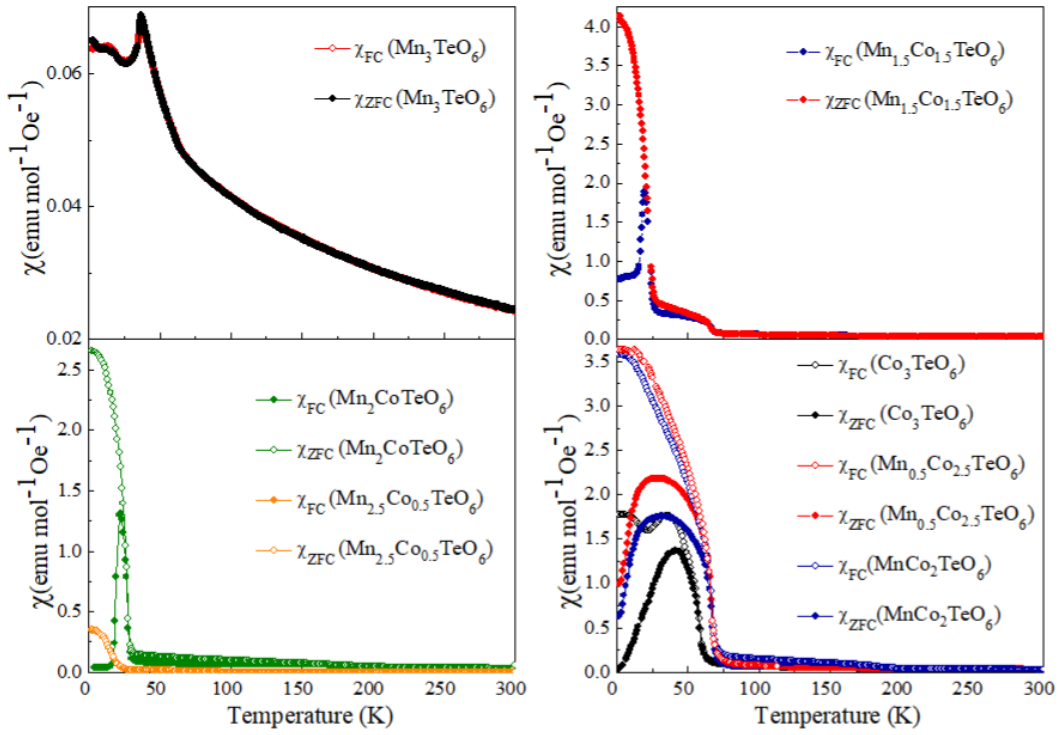

SF1. FC-ZFC curves for Mn3TeO6-II DPv (top left), $Mn_{3-x}Co_xTeO_6$-II x = 0.5, 1 (bottom left) DPv, x = 1.5 (top right) showing independent transitions for both polymorphs and x = 2, 2.5 and 3 NTO (bottom right).

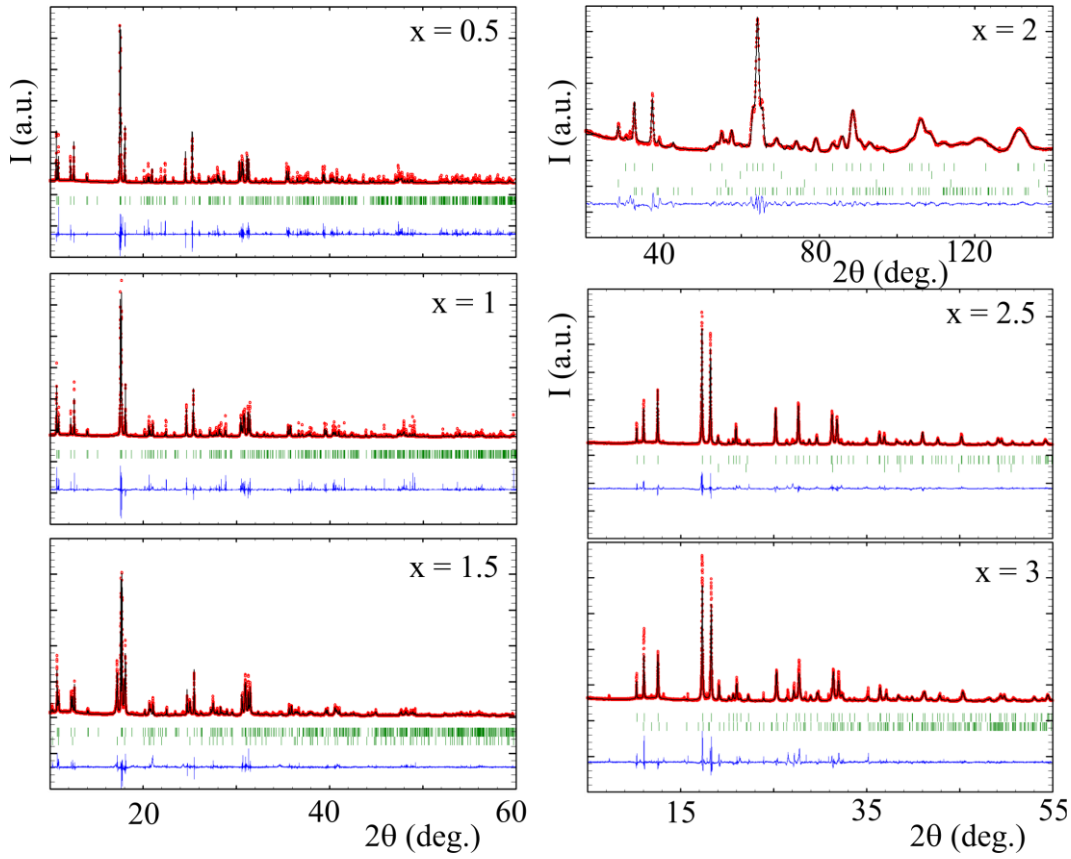

SF2. Rietveld fits to 300 K SXRD data for HP-$Mn_{3-x}Co_xTeO_6$ solid solution. No SXRD data are available for x = 2. Fit to 90 K NPD data are shown instead.

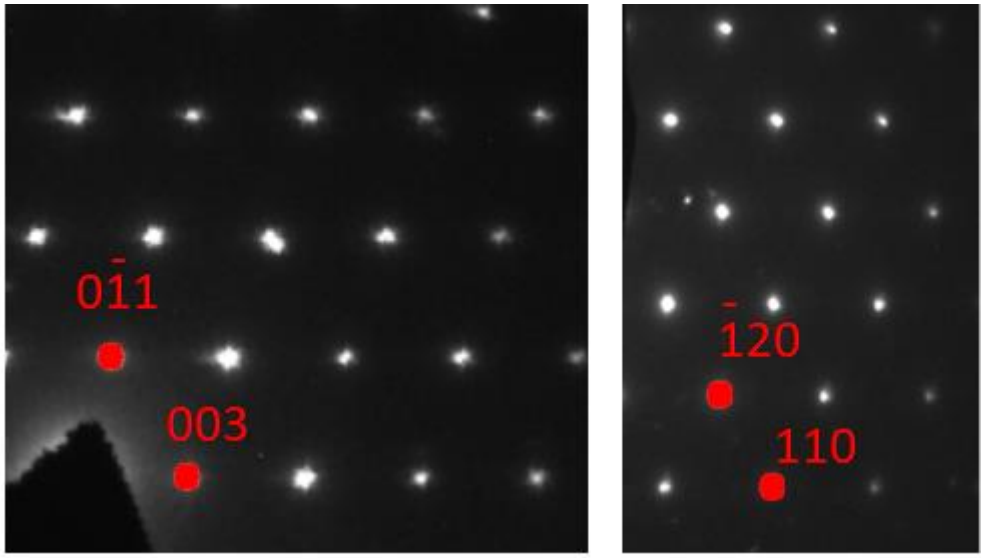

SF3. SAED from [1 0 0] and [0 0 1] of NTO-Co_3TeO_6. All diffraction maxima are indexed within the *R3* cell of NTO.

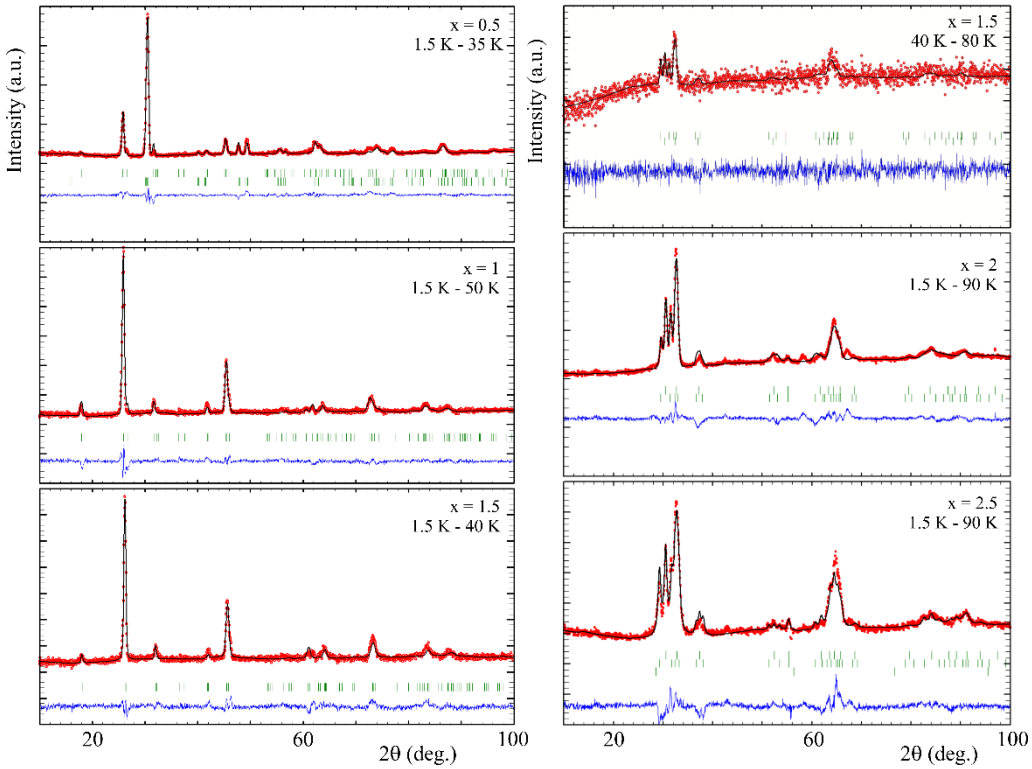

SF4. Rietveld fits to the NPD difference patterns for HP-$Mn_{3-x}Co_xTeO_6$ solid solution for magnetic structures determination.

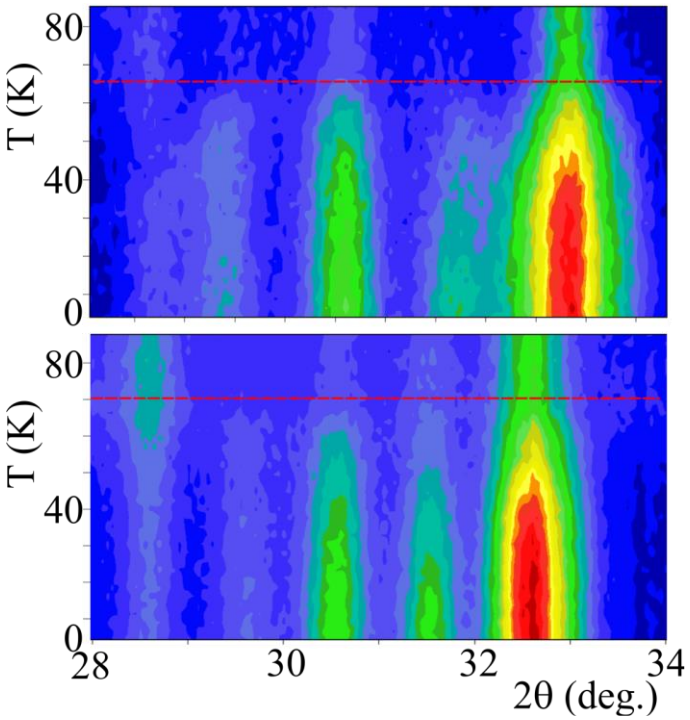

SF5. 2D NPD thermodiffraction for HP-$Mn_{0.5}Co_{2.5}TeO_6$ and HP-$MnCo_2TeO_6$ compounds. Dashed red line shows T_N. No thermal dependence of the propagation vectors is observed.

[1] R. D. Shannon, C. T. Prewitt, *Acta Cryst. B.* 1969, **25**, 925.
[2] J. Rodriguez-Carvajal, *Physica B*, 1993, **192**, 55.
[3] A.M. Arévalo-López, E. Solana-Madruga, C. Aguilar-Maldonado, C. Ritter, O. Mentré, J.P. Attfield, *Chem. Commun.* 2019, **55**, 14470-14473.